Factorial kriging for estimating and mapping the geochemical background from in situ gamma dose rate measurements downstream of a former uranium mine

Mathieu Le Coz, Alkiviadis Gourgiotis, Pascale Blanchart, Arnaud Mangeret

Factorial kriging for estimating and mapping the geochemical background from in situ gamma dose rate measurements downstream of a former uranium mine

Mathieu Le Coz[1], Alkiviadis Gourgiotis[1], Pascale Blanchart[1], Arnaud Mangeret[1]

[1]Institut de Radioprotection et de Sureté Nucléaire (IRSN), PSE-ENV/SEDRE, 31 avenue de la Division Leclerc, 92260, Fontenay-aux-Roses, France.

Highlights

- Factorial kriging allows to map the geochemical background component of gamma dose rate.
- Uranium mining activities impact gamma dose rate along drainage networks.
- Geostatistical analysis of radiometric data allows to better interpret localized geochemical results.

Abstract

A geostatistical approach is applied for extracting the geochemical background from gamma dose rate data acquired downstream of a former French uranium mining area. The exploratory data analysis shows that the spatial structure of the gamma dose rate consists of two components: a short isotropic component (10 m-range) that corresponds to the geochemical background; and a long anisotropic component (30 to 60 m-range) that corresponds to the drainage network features previously fed by the mine discharge water. The gamma dose rate on the whole area of interest was estimated and simulated (to deal with uncertainties) through a kriging of the measured values. The spatial component related to the geochemical background was then extracted through factorial kriging. The proportion of the gamma dose rate explained by the geochemical background according to factorial kriging is consistent within uncertainties with geochemical analyses performed on soil and sediment samples. This study thus highlights the potential of such geostatistical approaches for better exploiting radiometric data.

Keywords

Geostatistics; spatial component; radiometric data; geochemical data.

1. Introduction

Uranium naturally occurs in soils and sediments with concentrations highly variable in space depending on both primary sources, related to the geochemistry and mineralogy of bedrock, and secondary sources, related to changes or modification of radioelements distribution due to weathering and pedogenesis (Wilford et al., 1997; Ielsch et al., 2017). On the other hand, downstream of former uranium mining sites, the dissemination of radioactively-enriched material from past mining and milling activities may result in increased uranium concentrations, especially along watercourses and in lakes and wetlands (Strok and Smodis, 2010; Wang et al., 2013; Morin et al., 2016; Stetten et al., 2018). Identifying the potential sources of uranium, i.e., geochemical background versus mining activities, is a key element for the decision-making process, especially for defining the strategies of effective management and remediation of contaminated soils and sediments (Gourgiotis et al., 2020).

Uranium-ores lead to the production of radiogenic lead (Pb) with a specific isotope composition; stable Pb isotope ratios measured in soils and sediments can thus be used as a tracer of mining and milling activities (Munksgaard et al., 2003; Bollhöfer et al., 2006; Frostick et al., 2008; Frostick et al., 2011; Cuvier et al., 2016; Dang et al., 2018; Liu et al., 2018; Gourgiotis et al., 2020). Such a geochemical approach requires material sampling and advanced time-consuming laboratory analyses and can only be carried out a few locations. In situ radiometric measurements, especially through gamma-ray monitoring techniques, which are commonly used for radioelement mapping (IAEA, 2003; Cuvier et al., 2016), could be exploited so as to tie these geochemical data together into a more coherent interpretation at the scale of the area of interest. However, this involves establishing a relation between geochemical and radiometric data (Guagliardi et al., 2013; Nguyen et al., 2018), in other words, extracting the component of the radiometric data related to either the geochemical background or the mining activities.

In geostatistics, the combined effects of various scales of spatial variation of a given property result in a nested variogram structure (Bourennane et al., 2017). Methods such as factorial kriging (Matheron,

1982; Goovaerts, 1997; Wackernagel, 1998) can be then used for estimating and mapping each of the spatial components of the variogram (e.g., Bourennane et al., 2017; Du et al., 2017; Queiroz et al., 2008). This approach could be applied on radiometric measurements for extracting geochemical background or mining/milling activities components, provided they correspond to distinct spatial scales. In general, geostatistics are particularly suitable for exploiting radiometric data since their high spatial density lead to a robust estimation of variograms (Masoudi et al., 2019). The current study aims at assessing the potential of factorial kriging for distinguishing the sources of uranium downstream of a former mining area and to compare it with a geochemically-based approach.

2. Study area and data

In 2015, the French Institute for Radiological Protection and Nuclear Safety (IRSN) carried out a radiological survey downstream of the former uranium mine of Ty-Gallen, Brittany, France (Fig. 1a). In situ gamma dose rate measurements were acquired and soil samples were collected for geochemical laboratory studies.

2.1. The uranium mine of Ty-Gallen

The underground mine of Ty-Gallen is located in the granitic massif of Pontivy containing fine to medium-sized leucogranites interspersed by a large number of aplitic and pegmatitic veins (AREVA, 2014). The extraction of the Ty-Gallen deposits led to the production of 49 tons of uranium from 1963 to 1981. During the mining operations, underground mine water was pumped through a technical borehole and discharged and partly channeled up to a wetland located 300 m downstream. This wetland seasonally supplies the “Brulé” stream (Fig. 1).

2.2. Gamma dose rate

Gamma dose rate measurements were performed through a Saphymo 6150 ADB probe used with a Saphymo 6150 AD5 radiation meter. The radiation range of the probe was set from 5 to 10^6 $nSv.h^{-1}$, with a scanning energy from 23 keV to 7 MeV. The device was embedded into the MARCASSIN system

(a self-standing vehicle developed by IRSN) for recording gamma dose rate at 50 cm above the soil surface for 2480 locations from the outlet of the mining water to the wetland (Mangeret et al., 2018) (Fig. 1).

2.3. Stable lead isotope ratio measurements

Four soil cores were sampled, three (C2, C4, and C6) in the wetland and one (C1) on the edge of the related topographic depression (Fig. 1b). The cores were extracted using a steel hand corer equipped with 5 cm diameter PVC core tubes and had lengths varying between 30 and 55 cm. They were conditioned under anaerobic atmosphere immediately after coring and were stored in an anaerobic glovebox in the laboratory before analysis (Stetten et al., 2018). A chemical purification of the samples was done before Pb isotope ratio characterization ($^{204}Pb/^{207}Pb$, $^{206}Pb/^{207}Pb$, and $^{208}Pb/^{207}Pb$) which was performed using an Agilent 8800 ICP-MS/MS (Agilent Technologies, Tokyo, Japan). The Pb portion coming from the uranium ore (i.e., related to the mining and milling activities, ^{mine}Pb hereafter) in the sediments and soils of the wetland was estimated with the help of a reevaluated mixing model (Gourgiotis et al., 2020) (Table 1).

3. Theoretical considerations

In order to characterize the spatial components of the gamma dose rate data, a geostatistical approach based on factorial kriging was applied. This approach first involved the analysis of the spatial variability of the measured (i.e., sampled) dose rate and the estimation of the dose rate between the measurements (i.e., at unsampled locations).

3.1. Variographic analysis

The regionalized variable theory (Chiles and Delfiner, 2012) states that a variable in an area has both random and spatial properties that can be characterized by computing an experimental variogram from field sampling, such as:

$$\gamma(h) = \frac{1}{2N(h)} \sum_{i=1}^{N(h)} [Z_{i+h} - Z_i]^2 \qquad [1]$$

where $\gamma(h)$ is the experimental variogram for the lag distance h between pairs of sampled locations; $N(h)$ is the number of pairs separated by lag distance h; Z_i and Z_{i+h} are the values of the regionalized variable at the sampled locations i and $i+h$. The experimental variogram can then be fitted by an established model or a linear combination of established models.

3.2. Estimation with ordinary kriging

Ordinary kriging (Chiles and Delfiner, 2012) was developed for estimating the value of the regionalized variable at an unsampled location using a linear weighting of sampled values of the variable surrounding this location, generally within a neighborhood that corresponds to the variogram range, such as:

$$Z^*_{x0} = \sum_{j=1}^{n} \lambda_j Z_j \quad \text{with} \quad \sum_{j=1}^{n} \lambda_j = 1 \quad [2]$$

where Z^*_{x0} is the estimated value of the variable at the unsampled location x_0; n is the number of sampled values considered; λ_j is the weight for the sampled value Z_j. The weights are obtained by solving the ordinary kriging system, built based on the unbiasedness condition and the minimization of the error variance:

$$\begin{bmatrix} -\Gamma & u \\ u^t & 0 \end{bmatrix} \begin{bmatrix} \Lambda \\ \mu \end{bmatrix} = \begin{bmatrix} -\Gamma_0 \\ 1 \end{bmatrix} \quad [3]$$

where Γ is the $(n \times n)$ matrix of variograms between each pair of sampled locations; u is a $(n \times 1)$ vector of unit values; Λ is the $(n \times 1)$ vector of kriging weights; μ is a Lagrange multiplier; Γ_0 is the $(n \times 1)$ vector of variograms between the sampled locations and the target point (i.e., the unsampled location).

3.3. Factorial kriging

Factorial kriging (Goovaerts, 1997; Chiles and Delfiner, 2012) was developed based on the idea that the regionalized variable can be considered as a linear combination of two mutually orthogonal (i.e., independent) random variables, called scale components, in addition to the mean:

$$Z = Y^1 + Y^2 + m \qquad [4]$$

where Z is the regionalized variable; Y^1 and Y^2 are the centered (i.e., mean is zero) scale components; m is the mean of the variable. The variogram of the regionalized variable itself is thus a combination of the variograms characterizing the scale components:

$$\gamma(h) = \alpha\gamma^1(h) + \beta\gamma^2(h) \qquad [5]$$

where $\gamma^1(h)$ and $\gamma^2(h)$ are the experimental variograms of Y^1 and Y^2 for the lag distance h; α and β represents the relative contribution of γ^1 and γ^2 to the total variance. None of the scale components is directly observable but they can be estimated by solving the following system:

$$Y^{1*}_{x0} = \sum_{j=1}^{n} \lambda_j^1 Z_j \qquad [6]$$

$$\begin{bmatrix} -\Gamma^1 & u \\ u^t & 0 \end{bmatrix} \begin{bmatrix} \Lambda^1 \\ \mu^1 \end{bmatrix} = \begin{bmatrix} -\alpha.\Gamma_0^1 \\ 0 \end{bmatrix} \qquad [7]$$

where Y^{1*}_{x0} is the estimated value of the scale component Y^1 at the location x_0; λ_j^1 is the weight for the sampled value Z_j; Γ^1 is the $(n \times n)$ matrix of variograms of the scale component Y^1 between each pair of sampled locations; Λ^1 is the $(n \times 1)$ vector of kriging weights; μ^1 is a Lagrange multiplier for the scale component Y^1; Γ_0^1 is the $(n \times 1)$ vector of variograms of the scale component Y^1 between the sampled locations and the target point.

3.4. Implementation

In this study, the geostatistical analysis was implemented through the RGeostats R package (MINES ParisTech / ARMINES, 2020). The input data set consists of the gamma dose rate values, i.e., 2480 measurements and the corresponding spatial coordinates (X and Y).

For the whole geostatistical analysis, a Gaussian anamorphosis (Chiles and Delfiner, 2012) was applied for transforming the multivariate distribution of gamma dose rate measurements into a normal distribution. The (factorial) kriging results depicted in Sections 4.2 and 4.3 correspond to back-transformed data.

In addition, the (factorial) kriging were performed on a grid with 2.5 m spatial resolution. The input data set was thus subsampled based on a nearest neighbor method so as to remove duplicates in each grid mesh (790 measurements remained).

4. Geochemical background extraction

The geostatistical analysis performed on the gamma dose rate data allowed to identify and separate two main spatial components; and then to map the contribution of the component assumed to be related to the geochemical background.

4.1. Exploratory data analysis

The measured gamma dose rates range from 50 $nSv.h^{-1}$ to 1800 $nSv.h^{-1}$ and qualitatively appear to consist of two main groups of values (Fig. 2): the lowest values, below 200 $nSv.h^{-1}$, almost log-normally distributed (G1); and the highest values, related to a spread distribution with a poorly defined mode (G2). By fitting a multivariate log-normal model on the whole data set, the group G1 was estimated to correspond to 53% of the data with a mean value of 100 $nSv.h^{-1}$ and the group G2 to 47% of the data with a mean value of 500 $nSv.h^{-1}$ (Fig. 2).

Experimental variograms computed directionally from the Gaussian-transformed dose rate data exhibits different ranges (i.e., the distance at which a variogram reaches a sill) in various directions, indicating a geometric anisotropy of the related spatial features. Indeed, the range values appear to be maximal according to the N 125°E direction and minimal orthogonally, i.e., according to the N 35°E direction (Fig. 3). More precisely, the experimental variograms computed for both these directions were fitted by adjusting a spherical model with two scale components (Fig. 3) (Table 2): (i) a short isotropic component with 10 m range; and (ii) a large anisotropic component with 60 m range in N 125°E direction and 30 m range orthogonally. The part of the variance explained by the short scale component is about 40%. It should be noted that the gamma dose rate data were mainly acquired along approximatively N 125°E oriented lines (Fig. 1): this results in an undersampling in the orthogonal direction for long lag distances and bias in experimental variogram values (Fig. 3b).

4.2. Spatial estimation and simulation

Ordinary kriging was applied with the nested (i.e., two-component) variogram model for estimating the gamma dose rate at unsampled locations on a grid with 2.5 m spatial resolution (Fig. 4a). The resulting map shows relatively high gamma dose rates (>200 $nSv.h^{-1}$) from the mine outlet to the wetland, especially along two main N 120°E to N 145°E oriented structures that correspond to the drainage network (ditches) and within the wetland. The kriging standard deviation indicates high uncertainties regarding the extent of these high gamma dose rate areas, especially in the vicinity of the wetland (Fig. 4b).

In order to deal with these uncertainties, a turning-bands simulation algorithm (Lantuejoul, 2002) was applied on the same grid for generating 100 equiprobable realizations of the gamma dose rate field that are consistent with the variogram model (Fig. 5a). The number of realizations was fixed to 100 since increasing the number of realizations does not significantly impact the results presented below. This set of realizations can then be used, for example, to compute and map the probability of exceeding threshold values (Fig. 5b).

4.3. Spatial component separation

Based on both exploratory data analysis and the gamma dose rate spatial estimation, the following assumptions were formulated:

- the large anisotropic N 125°E-oriented spatial component identified in the variograms corresponds to the drainage network fed by the mine discharge water, and thus to the high gamma dose rate areas;
- the short isotropic component corresponds to the geochemical background, which can be characterized in terms of gamma dose rate values through the distribution G1 (i.e., mean value of 100 $nSv.h^{-1}$).

Factorial kriging was applied for separating the short isotropic component from the estimated gamma dose rate field. The mean of this component was set to 100 $nSv.h^{-1}$ and the resulting map (Fig 6a) was then compared to the estimations so as to compute the proportion of the gamma dose rate that is explained by the short spatial component, i.e., by the geochemical background (Fig. 6b). The short component appears to explain more than 75% of the estimated gamma dose rate on the major part of the domain, except along the drainage network of the mine water and in the wetland area.

In order to deal with kriging uncertainties, the same procedure was applied for each of the 100 realizations of the gamma dose rate simulated field. The results can be used, for example, to compute and map the probability of explaining a given proportion of the simulated gamma dose rate through the geochemical background (Fig. 7).

5. Assessment and discussion

The proportion of the gamma dose rate that is explained by the geochemical background according to the factorial kriging applied on the simulated fields was sampled at the core locations (C1, C2, C4 and C6, Fig 1b) and compared to the estimated percentages of Pb not related to the mining and milling activities (Table 1). These percentages are generally comprised between the 1^{st} and the 3^{rd} quartiles of the proportion of the gamma dose rate explained by the geochemical background (Fig. 8). Both radiometric- and geochemical-based approaches, based on strongly different measurements and processes, thus appear to lead to consistent results. Although a relevant assessment probably requires more comparison points spread over the whole investigated domain, such results are promising, especially when considering that the data were acquired during a single-shot survey without the aim of conducting a spatial analysis.

It should be noted that the depth of the field of view related to the sub-surface gamma dose rate induced by uranium decay products, especially ^{226}Ra (the long-lived parent of ^{214}Bi, which predominantly contributes to the measured gamma dose rate), is generally estimated to be about 25 cm below the ground surface (IAEA, 2003), with a major contribution of the radionuclides located in

the top few centimeters of soil (Varley et al., 2016). The interpretation of the gamma dose rate data thus ought to be limited to this depth. On the other hand, the mobility of ^{mine}Pb could differ from the mobility of uranium and ^{226}Ra, and the assumption of a codispersion in depth should be used with caution (Gourgiotis et al., 2020). In particular, a relative uranium or ^{226}Ra loss in top soil layers could result in a relative underestimation of the geochemical background contribution when using the radiometric-based approach (e.g., as for the 3 cm- and 10 cm-depth samples on core C4; Fig. 8). Discrepancy in estimated geochemical background proportions resulting from the two approaches could therefore be analyzed with respect to the sampling depth in order to better highlight differences in mobility of uranium and ^{mine}Pb at a site scale.

More broadly, this study confirms that in situ gamma dose rate measurements, often only considered as a way for performing a quick radiological screening of a domain during a reconnaissance phase, can be exploited for better characterizing the spatial variability of a contamination by radionuclides. The acquisition strategy, in terms of location and measurement devices, thus needs to be established based on this purpose. The geostatistical approach carried out in this study focuses on the analysis of a single variable, i.e., the gamma dose rate data. The use of secondary variables such as topography (or related variables that describe the drainage system), land use or geology could lead to reduce the uncertainties related to the estimations and simulations (e.g., Guastaldi et al., 2013; Warnery et al., 2015) and to reinforce the assumptions regarding the spatial components of the gamma dose rate data. In addition, gamma dose rate is linked to radio-isotopes that produce high-energy gamma rays, i.e., uranium (^{238}U and ^{235}U and their daughters) but also thorium (^{232}Th and its daughters) and potassium (^{40}K). A geostatistical analysis of the unfolded spectrum acquired by spectroscopy survey (e.g., Kaplan et al., 2020) by using factorial kriging into a multivariate framework (e.g., Imrie et al., 2008), could lead to better constraint the mapping of the component of the dose rate related to the mining/milling activities.

6. Conclusion

This study shows that factorial kriging can be used for extracting the component of radiometric data related to the geochemical background, and thus to link radiometric and geochemical data when both natural and anthropogenic sources of radionuclides occur with distinct spatial scales. The map of the geochemical background component deduced from radiometric data could be used either for guiding the sampling strategy of soil for geochemical analyses and/or for constraining the spatial interpolation of the localized background radionuclide concentrations (or its complementary, i.e., the concentrations attributable to anthropogenic source) estimated based on geochemical approaches.

Acknowledgments

This work was supported by IRSN. The authors are really grateful to owners of the wetland for the access to the site. . The authors would also like to thank the Charlotte Cazala, Christophe Debayle and Léa Pannecoucke (IRSN) for their suggested improvements to the manuscript.

References

AREVA. 2014. Bilan Environnemental - Sites miniers de la Bretagne - Départements du Finistère et du Morbihan (in French). AREVA, BG Mines / DRES / Direction de l'Après-Mines.

Bollhöfer, A., Honeybun, R., Rosman, K., Martin, P., 2006. The lead isotopic composition of dust in the vicinity of a uranium mine in northern Australia and its use for radiation dose assessment. Sci. Total Environ., 366 : 579-589. https://doi.org/10.1016/j.scitotenv.2005.11.016

Bourennane H., Hinschberger F., Chartin C., Salvador-Blanes S., 2017. Spatial filtering of electrical resistivity and slope intensity: Enhancement of spatial estimates of a soil property. J. Appl. Geophy., 138: 210-219. https://doi.org/10.1016/j.jappgeo.2017.01.032

Chiles J.P., Delfiner P. 2012. Geostatistics: modeling spatial uncertainty, 2nd Edition. Wiley series in probability and statistics, Wiley.

Cuvier, A., Pourcelot, L., Probst, A., Prunier, J., Le Roux, G., 2016. Trace elements and Pb isotopes in soils and sediments impacted by uranium mining. Sci. Total Environ., 566-567: 238-249. https://doi.org/10.1016/j.scitotenv.2016.04.213

Dang, D.H., Wang, W., Pelletier, P., Poulain, A.J., Evans, R.D., 2018. Uranium dispersion from U tailings and mechanisms leading to U accumulation in sediments: Insights from biogeochemical and isotopic approaches. Sci. Total Environ., 610-611: 880-891. https://doi.org/10.1016/j.scitotenv.2017.08.156

Du C., Liu E., Chen N., Wang W., Gui Z., He X. 2017. Factorial kriging analysis and pollution evaluation of potentially toxic elements in soils in a phosphorus-rich area, South Central China. J. Geochem. Explor., 175: 138-147. https://doi.org/10.1016/j.gexplo.2017.01.010

Frostick, A., Bollhöfer, A., Parry, D., 2011. A study of radionuclides, metals and stable lead isotope ratios in sediments and soils in the vicinity of natural U-mineralisation areas in the Northern Territory. J. Environ. Radioact. 102: 911-918. https://doi.org/10.1016/j.jenvrad.2010.04.003

Frostick, A., Bollhöfer, A., Parry, D., Munksgaard, N., Evans, K., 2008. Radioactive and radiogenic isotopes in sediments from Cooper Creek, Western Arnhem Land. J. Environ. Radioact., 99: 468-482. https://doi.org/10.1016/j.jenvrad.2007.08.015

Goovaerts P. 1997. Geostatistics for natural resources evaluation. Oxford University Press.

Gourgiotis A., Mangeret A., Manhes G., Blanchart P., Stetten L., Morin G., Le Pape P., Lefebvre P., Le Coz M., Cazala C. 2020. New insights into Pb isotope fingerprinting of U-Mine material dissemination in the environment: Pb isotopes as a memory dissemination tracer. Environ. Sci. Technol., 54(2): 797-806. https://doi.org/10.1021/acs.est.9b04828

Guagliardi I., Buttafuoco G., Apollaro C., Bloise A., De Rosa R., Cicchella, D. 2013. Using gamma spectrometry and geostatistics for assessing geochemical behaviour of radioactive elements in the lese catchment (southern Italy). Int. J. Environ. Res., 7(3): 645-658. https://doi.org/10.22059/ijer.2013.644

Guastaldi E., Baldoncini M., Bezzon G. et al. 2013. A multivariate spatial interpolation of airborne γ-ray data using the geological constraints. Remote Sen. Environ., 137: 1-11. https://doi.org/10.1016/j.rse.2013.05.027

IAEA. 2003. Guidelines for radioelement mapping using gamma ray spectrometry data. IAEA-TECDOC-1363, International Atomic Energy Agency.

Ielsch G., Cuney M., Buscail F., Rossi F., Leon A., Cushing M.E. 2017. Estimation and mapping of uranium content of geological units in France. J. Environ. Radioac., 166(2): 210-219. https://doi.org/10.1016/j.jenvrad.2016.05.022

Imrie C.E., Korre A., Munoz-Melendez G., Thornton I., Durucan S. 2008. Application of factorial kriging analysis to the FOREGS European topsoil geochemistry database. Sci. Total Environ., 393(1): 96-110. https://doi.org/10.1016/j.scitotenv.2007.12.012

Kaplan D.I., Smith R., Parker C.J., Baker M., Cabrera T., Ferguson B.O., Kemner K.M., Laird M., Logan C., Lott J., Manglass L., Martinez N.E., Montgomery D., Seaman J.C., Shapiro M., Powell B.A. 2020. Uranium attenuated by a wetland 50 years after release into a stream. ACS Earth Space Chem. 4(8): 1360-1366. https://doi.org/10.1021/acsearthspacechem.0c00124

Lantuejoul C. 2002. Geostatistical simulation - Models and algorithms. Springer-Verlag.

Liu, J., Luo, X., Wang, J., Xiao, T., Yin, M., Belshaw, N.S., Lippold, H., Kong, L., Xiao, E., Bao, Z.a., Li, N., Chen, Y., Linghu, W., 2018. Provenance of uranium in a sediment core from a natural reservoir, South China: Application of Pb stable isotope analysis. Chemosphere, 193: 1172-1180. https://doi.org/10.1016/j.chemosphere.2017.11.131

Mangeret, A., Blanchart, P., Alcalde, G., Amet, X., Cazala, C., Gallerand, M.O. 2018. An evidence of chemically and physically mediated migration of 238U and its daughter isotopes in the vicinity of a former uranium mine. J. Environ. Radioact., 195: 67–71. https://doi.org/10.1016/j.jenvrad.2018.08.018

Masoudi, P., Le Coz M., Cazala C., Saito K. 2019. Spatial properties of soil analyses and airborne measurements for reconnaissance of soil contamination by 137Cs after Fukushima nuclear accident in 2011. J. Environ. Radioact., 202: 74-84. https://doi.org/10.1016/j.jenvrad.2018.11.014

Matheron, G., 1982. Pour une analyse krigeante des données régionalisées (in French). Internal. Note N-732, Fontainebleau, Centre de Géostatistique.

MINES ParisTech / ARMINES (2020). RGeostats: The Geostatistical R Package. Version: 11.2.13. Free download from: http://cg.ensmp.fr/rgeostats.

Morin, G., Mangeret, A., Othmane, G., Stetten, L., Seder-Colomina, M., Brest, J., Ona-Nguema, G., Bassot, S., Courbet, C., Guillevic, J., Thouvenot, A., Mathon, O., Proux, O., Bargar, J. R. 2016. Mononuclear U(IV) complexes and ningyoite as major uranium species in lake sediments. Geochem. Perspect. Let., 2: 95-105. https://doi.org/10.7185/geochemlet.1610

Munksgaard, N.C., Brazier, J.A., Moir, C.M., Parry, D.L., 2003. The use of lead isotopes in monitoring environmental impacts of uranium and lead mining in Northern Australia. Aust. J. Chem., 56: 233-238. https://doi.org/10.1071/CH02239

Nguyen H.L., de Fouquet C., Courbet C., Gurriaran R., Kashparov V., Levchuk S., Barker E. 2018. Analysis of the relationship binding in situ gamma count rates and soil sample activities: Implication on radionuclide inventory and uncertainty estimates due to spatial variability. J. Environ. Radioact. 192: 349-361. https://doi.org/10.1016/j.jenvrad.2018.06.021

Queiroz J.C.B., Sturaro J.R., Saraiva A.C.F., Barbosa Landim P.M. 2008. Geochemical characterization of heavy metal contaminated area using multivariate factorial kriging. Environ. Geol., 55: 95-105. https://doi.org/10.1007/s00254-007-0968-3

Stetten L., Blanchart P., Mangeret A., Lefebvre P., Le Pape P. Brest J., Merrot P., Julien A., Proux O., Webb S.M., Bargar J.R., Cazala C., Morin G. 2018. Redox fluctuations and organic complexation govern

uranium redistribution from U(IV)-phosphate minerals in a mining-polluted wetland soil, Brittany, France. Environ. Sci. Technol., 52(22): 13099–13109. https://doi.org/10.1021/acs.est.8b03031

Strok M., Smodis B. 2010. Fractionation of natural radionuclides in soils from the vicinity of a former uranium mine Zirovski vrh, Slovenia. J. Environ. Radioact., 101: 22-28. https://doi.org/10.1016/j.jenvrad.2009.08.006

Varley A., Tyler A., Smith L., Dale P., Davies M. 2016. Mapping the spatial distribution and activity of ^{226}Ra at legacy sites through Machine Learning interpretation of gamma spectrometry data. Sci. Total Environ., 545-546: 654-661. https://doi.org/10.1016/j.scitotenv.2015.10.112

Wackernagel H. 1998. Multivariate Geostatistics. Springer-Verlag.

Wang Y., Frutschi M., Suvorova E., Phrommavanh V., Descostes M., Osman A.A., Geipel G., Bernier-Latmani R. 2013. Mobile uranium (IV)-bearing colloids in a mining-impacted wetland. Nat. Commun. 4: 2942. https://doi.org/10.1038/ncomms3942

Warnery E., Ielsch G., Lajaunie C., Cale E., Wackernagel H., Debayle C., Guillevic J. 2015. Indoor terrestrial gamma dose rate mapping in France: a case study using two different geostatistical models. J. Environ. Radioact., 139: 140-148. https://doi.org/10.1016/j.jenvrad.2014.10.002

Tables

Table 1. Proportion of lead (Pb) not related to the mining and milling activities (i.e. Pb attributable to the geochemical background) estimated based on geochemical analyses of soils and sediments sampled on the cores C1, C2, C4 and C6 (Fig. 1b) (from Gourgiotis et al., 2020).

Core	Depth (cm)	Geochemical background Pb (% of the total Pb)
C1	0-30	100
C2	5	51
	20	44
	25	42
	30	44
	40	98

	52	42
C4	3	30
	10	18
	15	39
	20	43
	25	46
C6	5.5	65
	10.5	52
	20.5	97
	38.5	39

Table 2. Parameters of the directional variogram models of the Gaussian-transformed gamma dose rate measurements according.

Direction	Component	Model type	Sill (% of the total variance)	Range (m)
N 125° E	Short	Spherical	40	12
	Long	Spherical	60	60
N 35°E	Short	Spherical	40	10
	Long	Spherical	60	30

Figures

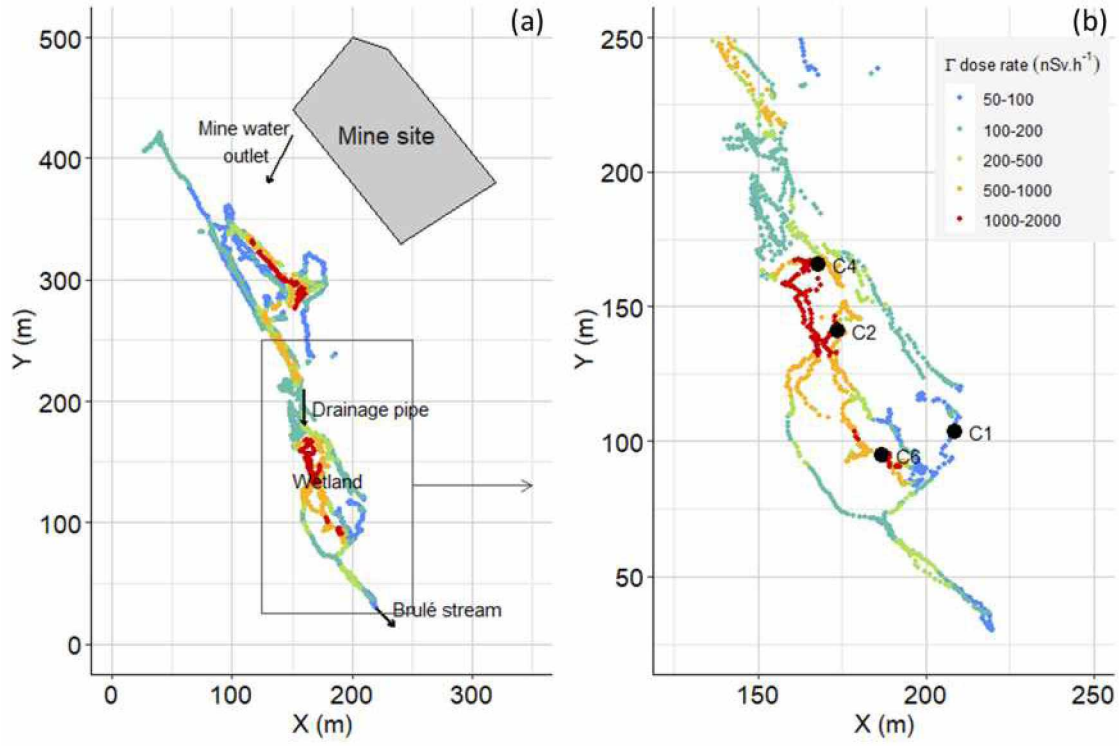

Fig. 1. Gamma dose rate measurements downstream of the Ty-Gallen mining area, Brittany, France (a); and location of cores C1, C2, C4 and C6 in the wetland area (b).

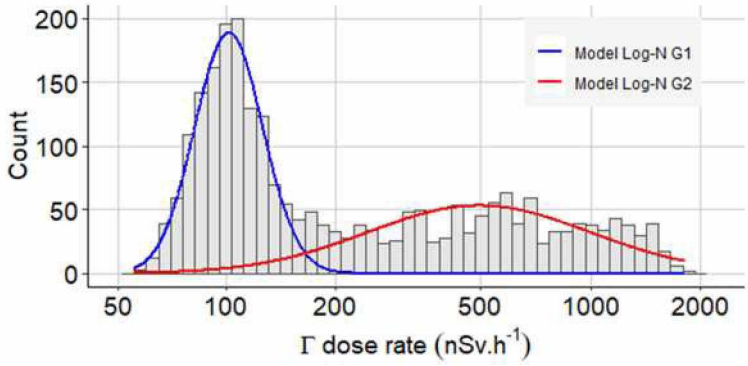

Fig. 2. Distribution of the gamma dose rate measurements and fitted components of a bivariate log-normal model (for groups of measurements G1 and G2).

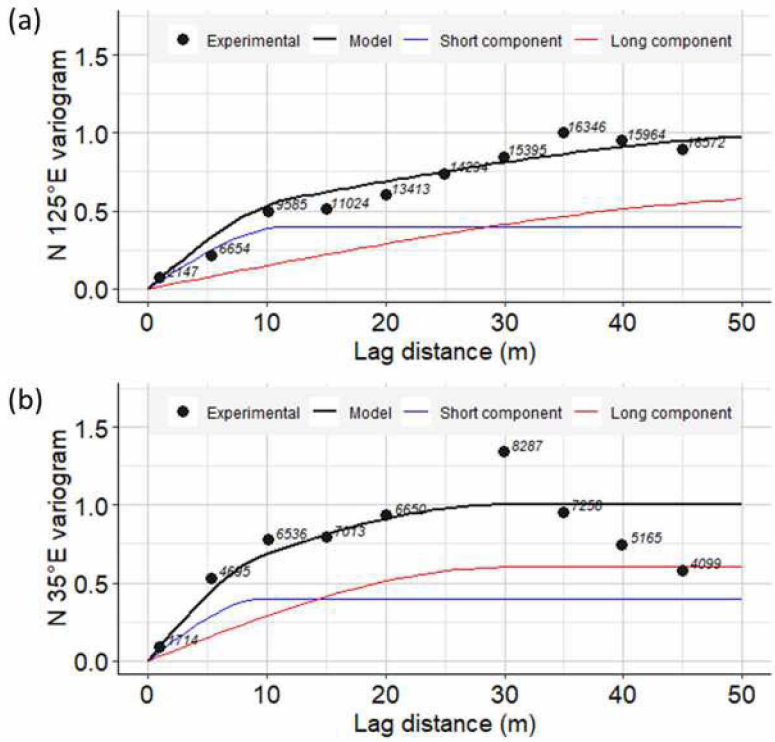

Fig. 3. Directional variograms (experimental and models) of the Gaussian-transformed gamma dose rate measurements according to N 125° E (a) and N 35°E (b) directions. The values in italics correspond to the number of pair of sampling used for computing the experimental variograms.

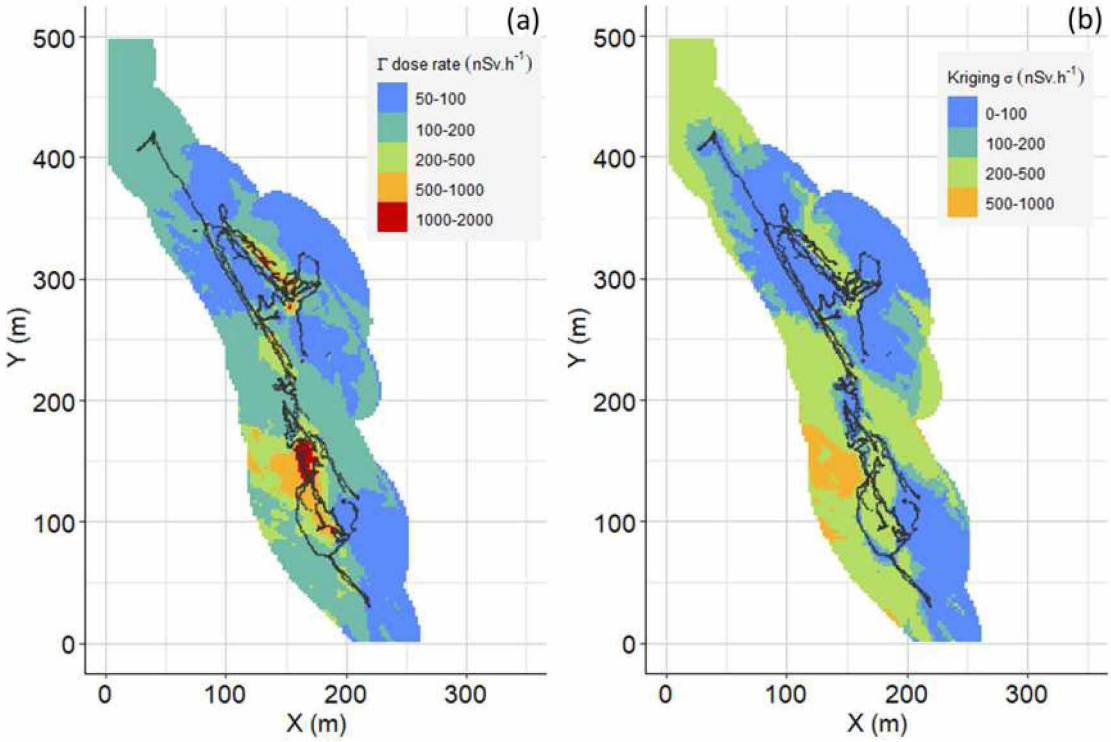

Fig. 4. Gamma dose rate field estimated by kriging of the measured values (a); and corresponding kriging standard deviation (b). The black dots correspond to the location of the measurements.

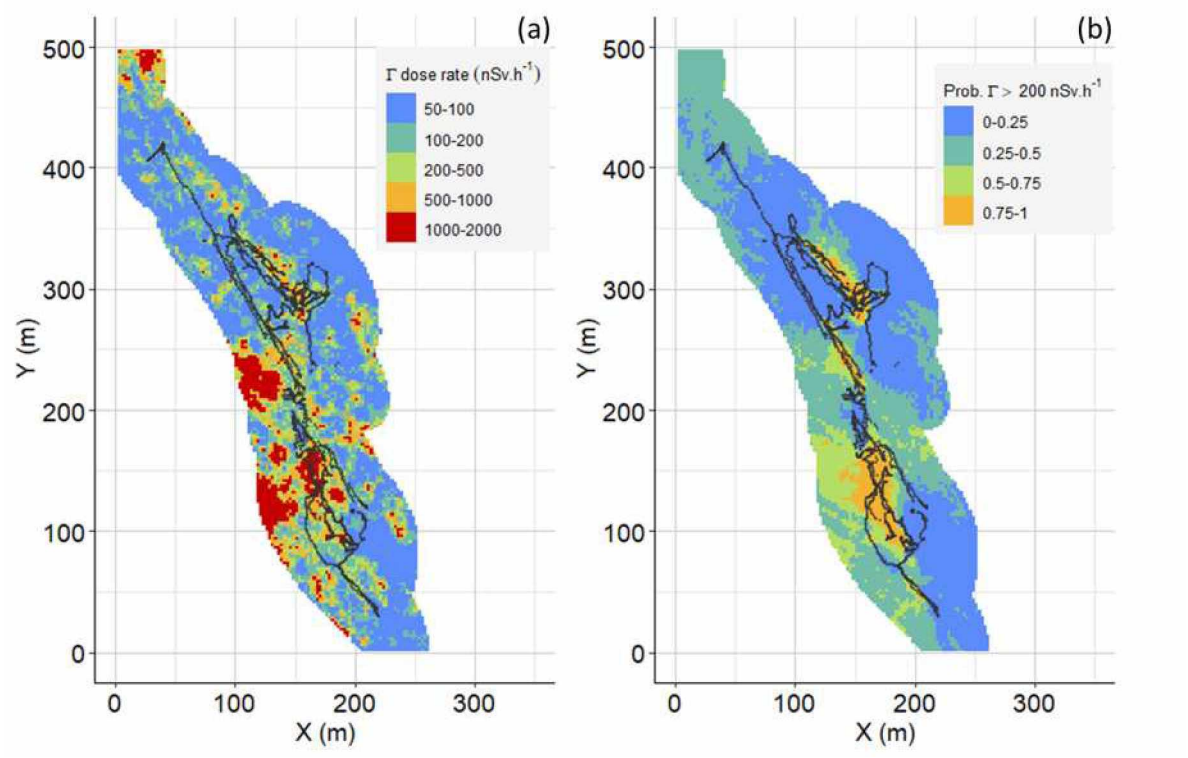

Fig. 5. One realization of a gamma dose rate field simulated by kriging of the measured values (a); and the probability of exceeding a gamma dose rate value of 200 $nSv.h^{-1}$, i.e., two times the geochemical background mean value (often considered to identify anthropic signal), computed based on 100 realizations (b). The black dots correspond to the location of the measurements.

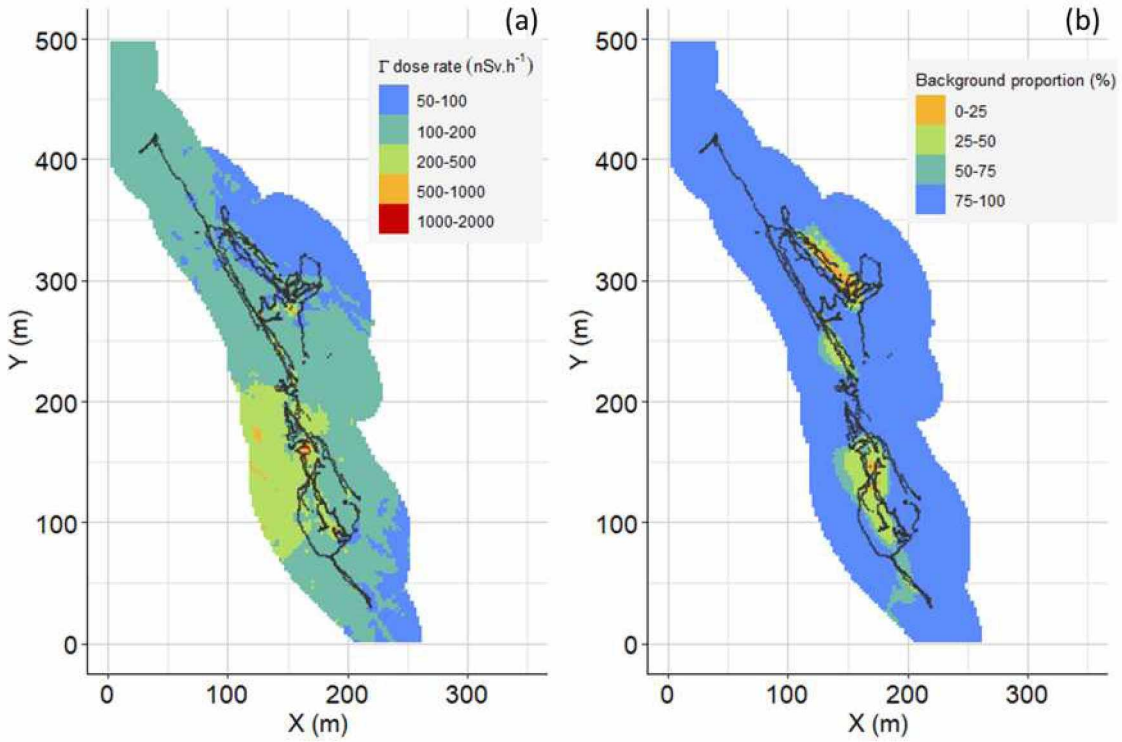

Fig. 6. Geochemical background component of the gamma dose rate estimated by factorial kriging of the total estimated gamma dose rate field (Fig. 4a) (a); and corresponding proportion of the total estimated gamma dose rate (b). The black dots correspond to the location of the measurements.

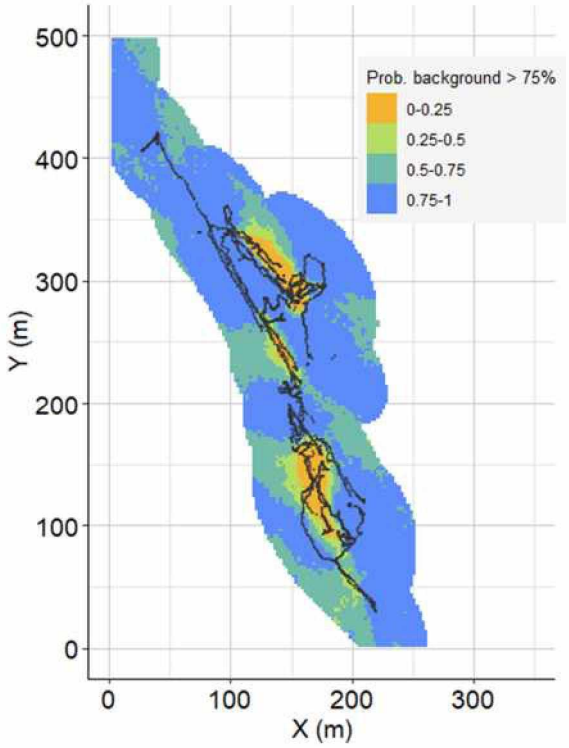

Fig. 7. Probability of explaining more than 75% of the total gamma dose rate by the geochemical background component. Map obtained based on factorial kriging of 100 realizations of the total simulated gamma dose rate field. The black dots correspond to the location of the measurements.

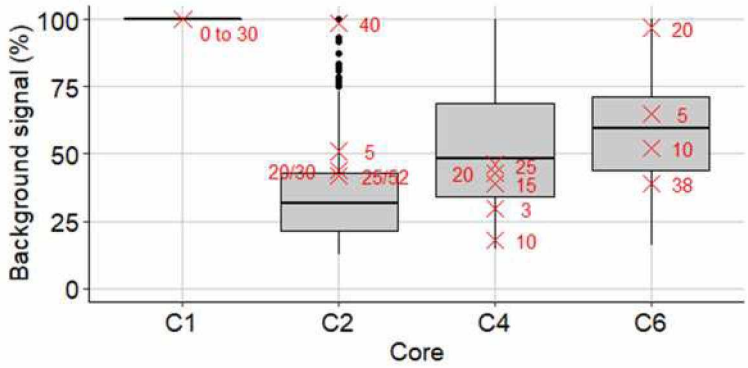

Fig. 8. Box-plots of the proportion of gamma dose rate explained by the geochemical background according to the factorial kriging applied on the simulated fields (100 realizations) at the core location. The red crosses correspond to the proportion of lead (Pb) not related to the mining and milling activities estimated based on geochemical analyses of core samples and the related values to the core depth in centimeters (Table 1; Gourgiotis et al., 2020).